Computer Assisted Mechanics and Engineering Sciences, **16**: 251–266, 2009.

Trefftz function for solving a quasi-static inverse problem of thermal stresses

Krzysztof Grysa, Artur Maciąg, Beata Maciejewska
Faculty of Management and Computer Modelling
Kielce University of Technology
Al. Tysiąclecia Państwa Polskiego 7,25-314 Kielce, Poland
e-mails: grysa@tu.kielce.pl, matam@tu.kielce.pl, beatam@tu.kielce.pl

(Received in the final form February 11, 2010)

The problem of thermal stresses in a hollow cylinder is considered. The problem is two-dimensional and the cross-section of the hollow cylinder is approximated as a long and thin rectangle as the ratio of the inner and outer radiuses is close to one. On the outer boundary of the hollow cylinder the heat source moves with a constant velocity. In the case of the rectangle the heat source moves on the upper side and the conditions of equality of temperatures and heat fluxes are assumed on the left and right boundaries. The stresses are to be found basing on the temperature measured inside the considered region, which means that an inverse problem is considered. Both for the temperature field and the displacements and stresses the finite element method is used. Thermal displacement potentials are introduced to find displacements and stresses. In order to construct the base functions in each element the Trefftz functions are used. For the temperature field the time-space finite elements are used and for the thermal displacement potentials the spatial elements are applied. Thanks to the use of the Trefftz functions a low-order approximation has given a solution very close to the exact one.

Keywords: Trefftz function, finite element method, thermal stresses, inverse problem, heat polynomials

1. Introduction

In the paper an approximate solution of the inverse problem of thermal stresses is presented. As the input data the internal temperature responses are used. The aim of this work is to explore the Trefftz functions [1] in this type of inverse problems.

Unlike other approximate methods the Trefftz method leads to an approximate solution that satisfies strictly the governing equation and approximately the initial and boundary conditions The method is flexible regarding the initial and boundary conditions. The conditions may be given in the discrete or continuous form, and they even may be incomplete. The obtained approximate solution is continuous with respect to all the variables. Trefftz functions can also be used as shape functions in FEM – the method is then called FEMT. Using FEMT we can built the time-space finite elements with base functions depending in continuous way on time and space variables and – as it is mentioned above – contrary to the classical FEM the obtained solution satisfies the governing equation. In addition, precision of the approximate solution can be improved not only by increasing the node number but also by increasing the degree of approximation. An important asset of the FEMT is the ability to solve inverse problems by using this method.

The concept of functions that satisfy a given differential equation and have to be fitted to the governing boundary conditions originates from Trefftz [1]. Trefftz functions (T-functions) for different linear partial differential equations are mainly used to construct an approximate solution of a given problem (a direct or an inverse one) in a form of linear combination of the functions. Such a solution satisfies the governing equation; in order to obtain the best fitting to the initial and boundary conditions a functional describing an inaccuracy of their fulfillment (error functional)

has to be minimized. In this way coefficients of the linear combination of heat polynomials are calculated.

A problem of thermal stresses identification based on temperature measured at inner points of a heated body belongs to the class of inverse problems of thermoelasticity.

T-functions in solving the inverse heat conduction problems have been presented in many papers, e.g., [2–4, 6–9]. Many examples of using T-function to identify boundary temperature, thermophysical coefficients or heat source density are presented in papers [11–17, 20, 21]. The inverse problems of elastokinetics and thermoelasticity has been also considered (cf. [10, 22–25] and a review [26]), but none of them used T-functions to find an approximate solution of the problem.

Because the T-functions fulfill the governing equations they are useful for constructing the base function in the FEM. In the paper a hollow cylinder with moving heat source along its lateral surface is considered. In order to find an approximate solution of the problem the Finite Element Method with T-functions (FEMT) used to construct the base functions is used [3, 17].

2. Problem formulation

Consider a homogeneous isotropic elastic hollow cylinder such that the ratio of its inner and outer radia is close to 1, i.e., $\frac{\bar{r}_w}{\bar{r}_z} \approx 1$. Assume that on the inner surface of the cylider a heat source moves in the angular direction with a constant velocity $\bar{v}_s$ (see Fig. 1). Additionally, assume that the heat source has constant density in both angular and radial directions so that the heat flow in the axial direction may be neglected. Such assumptions allow to consider the problem as a 2D one in a ring-shaped area (see Fig. 2).

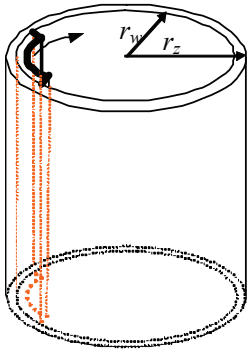

Fig. 1. A hollow circular cylinder

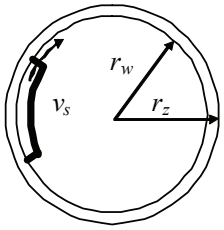

Fig. 2. A circular ring

The assumption $\frac{\bar{r}_w}{\bar{r}_z} \approx 1$ makes it possible to "unroll" the ring and to consider a rectangular area with height much smaller than length. On both ends of such rectangle the IV kind boundary conditions have to be satisfied and the heat source is assumed to move along the upper side of the rectangle periodically with constant velocity (see Fig. 3).

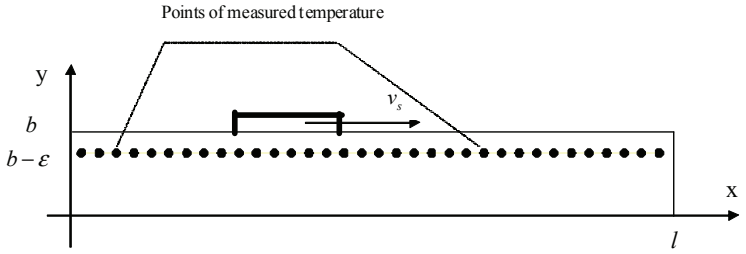

Fig. 3. The rectangle which models the ring with moving heat sources on its inner side

The temperature is measured in chosen set of points close to the upper side of the rectangle (on which the heat source is moving). The lower side of the body is assumed to be thermally insulated. The problem may be considered now as a 2D one.

As a result of heating a body the thermal stresses arise. The accepted assumptions lead to the conclusion that the normal stress in the axial direction in the cylinder (in rectangle in the z-axis direction) $\bar{\sigma}_z$ and the tangential stresses $\bar{\tau}_{xz}$, $\bar{\tau}_{yz}$ are zero, which means that the plane stress state is considered. Moreover, we assume that the boundary of the cylinder (of the rectangle) is free of stresses.

The problem is formulated and solved in the dimensionless coordinates but all numerical results are presented dimensionally.

At first the temperature field has to be determined. Then, in the system of displacement equations that describes the plane stress state the thermal term appears on the right-hand side as a source term. The problem is described mathematically as follows:

$$\frac{\partial^2 T}{\partial x^2} + \frac{\partial^2 T}{\partial y^2} - \frac{\partial T}{\partial t} = 0 \quad \text{for } (x,y) \in \Omega,\ t > 0, \tag{1}$$

with $\Omega = \{(x,y):\ 0 < x < l,\ 0 < y < b\}$,

$$(1-\nu)\frac{\partial^2 U}{\partial x^2} + \frac{\partial^2 U}{\partial y^2} + (1+\nu)\frac{\partial}{\partial x}\Big(\frac{\partial U}{\partial x} + \frac{\partial V}{\partial y}\Big) = \frac{\partial T}{\partial x}, \tag{2}$$

$$(1-\nu)\frac{\partial^2 V}{\partial x^2} + \frac{\partial^2 V}{\partial y^2} + (1+\nu)\frac{\partial}{\partial y}\Big(\frac{\partial U}{\partial x} + \frac{\partial V}{\partial y}\Big) = \frac{\partial T}{\partial y} \quad \text{for } 0 \le x \le l,\ 0 \le y \le b, \tag{3}$$

$$T(x,y,0) = 0, \tag{4}$$

$$\frac{\partial T}{\partial y}(x,0,t) = 0, \quad T(0,y,t) = T(l,y,t), \quad \frac{\partial T}{\partial x}(0,y,t) = \frac{\partial T}{\partial x}(l,y,t), \tag{5}$$

$$\sigma_y(x,0,t) = 0, \tau_{xy}(x,0,t) = 0, \quad \sigma_y(x,b,t) = 0, \tau_{xy}(x,b,t) = 0, \tag{6}$$

$$U(0,y,t) = U(l,y,t), \quad V(0,y,t) = V(l,y,t), \tag{7}$$

$$\sigma_x(0,y,t) = \sigma_x(l,y,t), \quad \sigma_y(0,y,t) = \sigma_y(l,y,t), \quad \tau_{xy}(0,y,t) = \tau_{xy}(l,y,t), \tag{8}$$

$$T(x_p,y_p,t_p) = W_p, \quad \text{for } p = 1,2,\dots P. \tag{9}$$

Here, W_p denotes the measured temperature value in (x_p,y_p,t_p), P is the number of points with measured temperature. The measurements are simulated from the exact solution (11) and disturbed with a noise with normal distribution not greater than 5% of the exact value. The formula (11) presents the exact solution of the problem (1), (4), (5), (10) where the condition (10) reads:

$$\frac{\partial T}{\partial y}(x,b,t) = \begin{cases} 0 & \text{for } x - v_s t \le 0, \\ Q\, f(x,t) & \text{for } 0 \le x - v_s t \le a, \\ 0 & \text{for } a \le x - v_s t \le l. \end{cases} \tag{10}$$

Here, $f(x,t) = (2/a)^4((x-v_s t) \bmod l - a)^2\big((x-v_s t) \bmod l\big)^2$, Q is a dimensionless quantity equal to the extreme value of density of heat flux ($Q > 0$), and $(x-v_s t) \bmod l = (x-v_s t)/l - \mathrm{Int}\,\big((x-v_s t)/l\big)$.

The solution of the problem (1), (4), (5), (10) has the form [18]:

$$
\begin{aligned}
T(x,y,t) = {} & \frac{q_0 t}{bl} + \frac{2}{bl}\sum_{k=1}^{\infty}\frac{(-1)^k q_0 \cos\alpha_k y}{\alpha_k^2}(1-e^{-\alpha_k^2 t}) \\
& + \frac{2}{bl}\sum_{n=1}^{\infty}\frac{q_{n1}\cos\gamma_{n0}}{\lambda_n^2}\Big(\cos(\lambda_n(x-v_s t)+\gamma_{n0}) - e^{-\lambda_n^2 t}\cos(\lambda_n x+\gamma_{n0})\Big) \\
& + \frac{4}{bl}\sum_{n=1}^{\infty}\sum_{k=1}^{\infty}\frac{(-1)^k q_{n1}\cos\gamma_{nk}\,\cos\alpha_k y}{\lambda_n^2+a_k^2}\Big(\cos(\lambda_n(x-v_s t)+\gamma_{nk}) \\
& \qquad - e^{-(\lambda_n^2+a_k^2)\,t}\cos(\lambda_n x+\gamma_{nk})\Big).
\end{aligned}
\tag{11}
$$

Here,

$$
\cos\gamma_{nk} = \frac{\alpha_k^2+\lambda_n^2}{\sqrt{v_s^2\lambda_n^2+(\alpha_k^2+\lambda_n^2)^2}}, \quad \lambda_n = \frac{2\,\pi\,n}{l}, \quad \alpha_k = \frac{k\,\pi}{b}, \quad n = 1,2,3,\ldots, \quad k = 0,1,2\ldots,
$$

$$
q_0 = \frac{8\,Q\,a}{15}, \quad q_{n1} = -\frac{8\,Q\,l^3\cos n\pi(3a\,l\,n\pi\cos\frac{an\pi}{l} + (a^2n^2\pi^2-3l^2)\sin\frac{an\pi}{l})}{a^4n^5\pi^5}.
$$

The dimensionless quantities are defined as follows:

$$
\{x;y;a;b;l\} = \frac{\{\bar{x};\bar{y};\bar{a};\bar{b};\bar{l}\}}{\bar{d}}, \quad t = \frac{\kappa\,\bar{t}}{\bar{d}^2}, \quad v_s = \frac{\bar{v}_s\,\bar{d}}{\kappa}, \quad T = \frac{\bar{T}-\bar{T}_0}{\frac{\bar{q}\,\bar{d}}{\bar{\lambda}}}, \quad \{U;V\} = \frac{\{\bar{U};\bar{V}\}}{\frac{\bar{q}\bar{d}^2\gamma}{\bar{\lambda}}},
$$

$$
\{\varepsilon_x;\varepsilon_y;\gamma_{xy}\} = \frac{\{\bar{\varepsilon}_x;\bar{\varepsilon}_y;\bar{\gamma}_{xy}\}}{\frac{\bar{q}\bar{d}\gamma}{\bar{\lambda}}}, \quad \{\sigma_x;\sigma_y\} = \frac{\{\bar{\sigma}_x;\bar{\sigma}_y\}}{\frac{\bar{q}\bar{d}\gamma}{\bar{\lambda}}\,\frac{2\mu}{1-\nu}}, \quad \tau_{xy} = \frac{\bar{\tau}_{xy}}{2\frac{\bar{q}\bar{d}\gamma}{\bar{\lambda}}\mu},
$$

where $(\bar{})$ denotes a quantity with dimension.

3. Temperature identification using FEMT

In order to find the temperature field in the considered region we use FEMT. To solve the problem described by Eqs. (1), (4), (5) and (9), the time-space region $\Omega\times <0,t_k>$ is divided on cuboid subregions. The area Ω is divided into small rectangles Ω_j , $j = 1,2,3,\ldots,J$. The time interval $<0,t_k>$ is divided into subintervals $<r\,\Delta t,(r+1)\Delta t>$ for $r = 0,1,2,\ldots,R$. An approximate solution of Eq. (1) in each time-space element $\bar{\Omega}_j = \Omega_j \times <t_0, t_0+\Delta t>$, $t_0 = r\Delta t$ for fixed r has the following form:

$$
\tilde{T}_j(x,y,t) = \sum_{n=1}^{N} A_{jn} v_n(\hat{x},\hat{y},\hat{t}) \tag{12}
$$

where $\hat{x} = x - x_{0j}$, $\hat{y} = y - y_{0j}$, and $\hat{t} = t - t_{0j}$; moreover, (x_{0j}, y_{0j}, t_{0j}) is an arbitrary but fixed point in $\bar{\Omega}_j$, $v_n(\hat{x},\hat{y},\hat{t})$ denotes the T-functions (heat polynomials), and A_{jn} stands for coefficients to be found.

To solve the equation (1) a method being a generalization of the one presented in [3] is used. The equation (1) is solved sequentially in the successive time intervals.

Consider a system of algebraic equations

$$
\tilde{T}_j(x_k,y_k,t_k) = \tilde{T}_{jk} = \sum_{n=1}^{N} A_{jn} v_n(\hat{x}_k,\hat{y}_k,\hat{t}_k), \quad k = 1,2,\ldots N. \tag{13}
$$

with (x_k, y_k, t_k) standing for coordinates of nodes of the element $\bar{\Omega}_j$, $j = 1, 2, 3, \ldots, J$. In the matrix form it reads

$$\mathbf{T} = \mathbf{v}\,\mathbf{A}. \tag{14}$$

Hence, after inverting the matrix $\mathbf{v}$ we obtain

$$\mathbf{A} = \mathbf{v}^{-1}\,\mathbf{T} = \mathbf{V}\,\mathbf{T}, \quad A_{jn} = \sum_{k=1}^{N} V_{nk}\tilde{T}_{jk}, \tag{15}$$

and finally

$$\tilde{T}_j(x,y,t) = \sum_{n=1}^{N}\left(\sum_{k=1}^{N} V_{nk}\tilde{T}_{jk}\right) v_n(\hat{x},\hat{y},\hat{t}) = \sum_{k=1}^{N}\left(\sum_{n=1}^{N} V_{nk} v_n(\hat{x},\hat{y},\hat{t})\right)\tilde{T}_{jk} = \sum_{k=1}^{N}\varphi_{jk}(x,y,t)\,\tilde{T}_{jk}. \tag{16}$$

Here,

$$\varphi_{jk}(x,y,t) = \sum_{n=1}^{N} V_{nk} v_n(\hat{x},\hat{y},\hat{t}) \tag{17}$$

is a base function for FEMT. The base function fulfills Eq. (1).

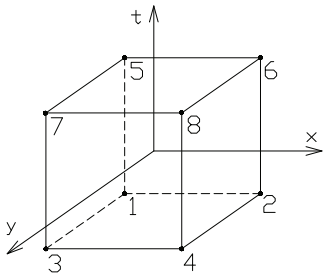

Fig. 4. The nodes in the finite time-space element

In $\bar{\Omega} = \Omega \times < t_0, t_0 + \Delta t >$ a rectangular net with lines parallel to the axes the system of coordinates is introduced as a result of dividing the sides of the considered rectangle on L_1 or L_2 parts in OX and OY directions, respectively. In each cuboid element $\bar{\Omega}_j$ eight nodes are chosen (see Fig. 4). Hence, in $\bar{\Omega}$ we have $2(L_1+1)(L_2+1)$ nodes. The base functions are linear combination of the heat polynomials (T-functions), written in local (in an element) system of coordinates as follows:

$$1, \quad \hat{x}, \quad \hat{y}, \quad \hat{x}\,\hat{y}, \quad \frac{\hat{y}^2}{2} + \hat{t}, \quad \frac{\hat{x}\,\hat{y}^2}{2} + \hat{x}\,\hat{t}, \quad \frac{\hat{y}^3}{6} + \hat{y}\,\hat{t}, \quad \frac{\hat{x}\,\hat{y}^3}{6} + \hat{x}\,\hat{y}\,\hat{t}.$$

Each node has its global number (resulting from numerating all nodes in $\bar{\Omega}$) and a local one (numeration in an element $\bar{\Omega}_j$).

The temperature in each 8-nodal element reads

$$\tilde{T}_j(x,y,t) = \sum_{k=1}^{l_w}\varphi_{jk}(x,y,t)\,\tilde{T}^n \quad \text{for } j = 1, 2, \ldots, (L_1\,L_2), \tag{18}$$

where j denotes the element number, l_w is the number of nodes in an element, k stands for the node number in j-th element, n is the node global number (in $\bar{\Omega}$), and $\tilde{T}^n$ stands for temperature value in the n-th node.

To find the unknown coefficients of the linear combination (18) one minimizes a functional J. The functional expresses a mean square error of the approximate solution with respect to boundary and initial conditions as well as the difference between heat fluxes between the neighbouring elements. The considered initial boundary problem is solved sequentially in the time interval $< r\,\Delta t, (r+1)\Delta t >$ for $r = 0, 1, 2, \ldots, R$.

The functional J has the following form:

$$
\begin{aligned}
J = &\sum_i \iint\limits_{D_1^i} \Big(\tilde{T}_{l_i}(x,y,t_0) - T_{0r}\Big)^2 dx\,dy + \sum_i \iint\limits_{D_2^j} \Big(\frac{\partial \tilde{T}_{l_i}}{\partial y}(x,0,t)\Big)^2 dx\,dt \\
&+ \sum_i \iint\limits_{D_3^i} \Big(\tilde{T}_{l_i}(0,y,t) - \tilde{T}_{k_i}(l,y,t)\Big)^2 dy\,dt + \sum_i \iint\limits_{D_3^l} \Big(\frac{\partial \tilde{T}_{l_i}}{\partial y}(0,y,t) - \frac{\partial \tilde{T}_{k_i}}{\partial y}(l,y,t)\Big)^2 dy\,dt \\
&+ \sum_i \sum_j \iint\limits_{D_4^{i,j}} \Big(\frac{\partial \tilde{T}_{l_i}}{\partial x}(x_j,y,t) - \frac{\partial \tilde{T}_{k_i}}{\partial x}(x_j,y,t)\Big)^2 dy\,dt \\
&+ \sum_i \sum_j \iint\limits_{D_5^{i,j}} \Big(\frac{\partial \tilde{T}_{l_i}}{\partial y}(x,y_j,t) - \frac{\partial \tilde{T}_{k_i}}{\partial y}(x,y_j,t)\Big)^2 dx\,dt + \sum_p \Big(\tilde{T}(x_p,y_p,t_p) - W_p\Big)^2
\end{aligned}
\tag{19}
$$

with D_i standing for a finite element and T_{0r} denoting an initial temperature value in r-th time interval, $r = 0, 1, 2, \ldots, R$ (it is the same as the final value of temperature in the previous time interval). For $r = 0$ the initial condition is given by formula (4).

After finding the approximate temperature field in the domain $\Omega \times < 0, t_k >$, the displacement equations (2), (3) are considered.

Solving numerically the problem of temperature field we divide the time-space domain onto 400 ($L_1 = 40$, $L_2 = 10$) and 800 ($L_1 = 80$, $L_2 = 10$) 8-nodal cuboid finite elements with nodes in the vertices. With 400 elements we have 902 nodes in the time-space domain; with 800 elements the number of nodes is equal to 1782. The points with simulated measurement of temperature are placed in the nodes on two levels in the distance, respectively, 0.003 m and 0.006 m from the surface with the moving heat source. The number of the measuring points depends on the number of finite elements. For 400 elements the number of measuring points is 82; for 800 elements it is equal 162.

Calculations have been made for six first time intervals. The time step is constant and equals $\Delta t = 0.378$ s. The simulated measurements generated from the exact solution are encumbered with noise with normal distribution, not exceeding 5% of the exact value of temperature. The approximate and exact solutions are compared at moments at the end of time intervals. The relative error is calculated according to the formula

$$
\text{rel. error} = \sqrt{\frac{\sum_{k=1}^{L} \Big(\tilde{T}(x_k,y_k,t_k) - T(x_k,y_k,t_k)\Big)^2}{\sum_{k=1}^{L} \big(T(x_k,y_k,t_k)\big)^2}}. \tag{20}
$$

Here, $\tilde{T}(x,y,t)$ is the approximate temperature, $T(x,y,t)$ denotes its exact value, L stands for the number of nodes, (x_k, y_k, t_k) are time-space coordinates of the nodes. The following data have been accepted for numerical calculations: $\bar{v}_s = 0.02$ m/s, $\bar{T}_0 = 293$ K, $\lambda = 45$ W/m K, $\bar{l} = 0.3$ m, $\bar{b} = 0.03$ m, $\bar{a} = 0.09$ m, $\kappa = 0.119 \cdot 10^{-4}$ m^2/s, $Q = 13 \cdot 10^4$. The results concerning temperature field after six time steps are presented in Fig. 5. The inaccuracy of the approximate solution is very small. In both cases the greatest value of temperature is 308.3 K. The relative error of temperature in the final moment of time interval is shown in Table 1.

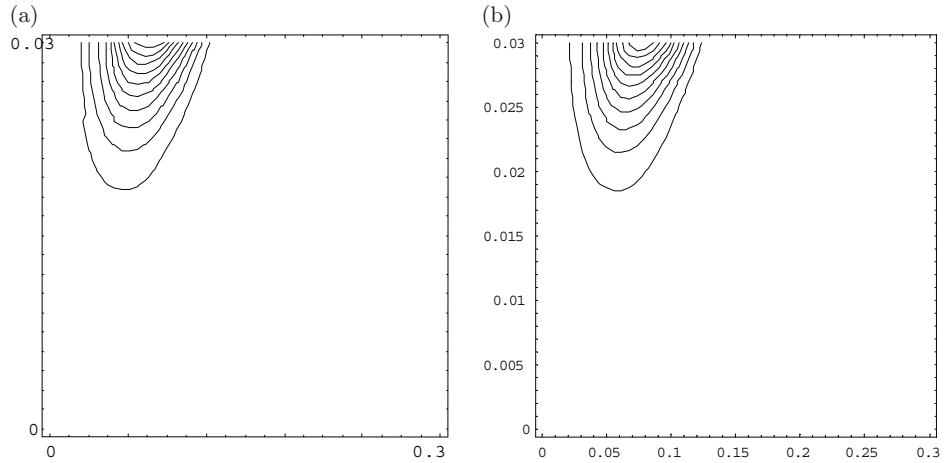

Fig. 5. Approximate (a) and exact (b) temperature field for $\bar{t} = 2.27$ s (for the approximation the domain was divided onto 800 elements)

Table 1. Relative error of temperature in the final moment of time interval

Time, $\bar{t}$ [s]	Relative error [%], Eq. (20)	
	400 elements $L = 902$	800 elements $L = 1782$
0.378	10.9	10.8
0.756	8.2	8.4
1.134	5.5	5.7
1.512	3.3	3.9
1.89	4.0	3.2
2.268	4.0	3.5

4. Thermal stresses

In order to determine thermal stresses the Lamé method is applied. The displacement system of equations (2), (3) is separated by using the thermal displacement potential functions [19]. In this approach the displacement vector is split into two parts as follows:

$$[U, V, 0] = \operatorname{grad} \Phi + \operatorname{rot} \boldsymbol{\Psi}. \tag{21}$$

Here, $\Phi = \Phi(x, y)$ and $\boldsymbol{\Psi} = [0, 0, \Psi]$ are the thermal displacement potential functions. Hence,

$$U = \frac{\partial \Phi}{\partial x} + \frac{\partial \Psi}{\partial y}, \quad V = \frac{\partial \Phi}{\partial y} - \frac{\partial \Psi}{\partial x}. \tag{22}$$

As a result for fixed $t = \tau$ two Poisson equations are obtained:

$$\nabla^2 \Phi(x, y) = h_1(x, y, \tau) + T(x, y, \tau), \tag{23}$$

$$\nabla^2 \Psi(x, y) = h_2(x, y, \tau), \tag{24}$$

with $T(x, y, t)$ standing for temperature. The functions $h_1(x, y, t)$, $h_2(x, y, t)$ have the following form:

$$h_1(x, y, t) = \frac{1}{l} h_{10}(y) + \frac{2}{l} \sum_{n=1}^{\infty} \big(h_{11n}(y) \cos \lambda_n (x - vt) + h_{12n}(y) \sin \lambda_n (x - vt) \big), \tag{25}$$

$$h_2(x,y,t)=\frac{1}{l}h_{20}(y)+\frac{2}{l}\sum_{n=1}^{\infty}\big(h_{21n}(y)\cos\lambda_n(x-vt)+h_{22n}(y)\sin\lambda_n(x-vt)\big), \tag{26}$$

where

$$h_{1n1}=A_{1n1}e^{\lambda_n y}+B_{1n1}e^{-\lambda_n y},\quad h_{1n2}=A_{1n2}e^{\lambda_n y}+B_{1n2}e^{-\lambda_n y},$$
$$h_{2n1}=\frac{2}{v-1}A_{1n2}e^{\lambda_n y}-\frac{2}{v-1}B_{1n2}e^{-\lambda_n y},\quad h_{2n2}=-\frac{2}{v-1}A_{1n1}e^{\lambda_n y}+\frac{2}{v-1}B_{1n1}e^{-\lambda_n y},$$
$$h_{01}=A_{01},\quad h_{02}=A_{02},\quad A_{01}=0,\quad A_{02}=0,$$

$$A_{1n1}=\frac{1-e^{b\lambda_n}}{-1+e^{2b\lambda_n}+2be^{b\lambda_n}\lambda_n}\frac{2(-1+\nu)\alpha_{1n0}}{(1+\nu)}$$
$$-\sum_{k=1}^{\infty}\left(\frac{(-1)^k e^{b\lambda_n}(-1+e^{2b\lambda_n}+2b\lambda_n)}{(1-e^{2b\lambda_n})^2-4b^2e^{2b\lambda_n}\lambda_n^2}+\frac{1-e^{2b\lambda_n}-2be^{2b\lambda_n}\lambda_n}{(1-e^{2b\lambda_n})^2-4b^2e^{2b\lambda_n}\lambda_n^2}\right)\frac{2(-1+\nu)\lambda_n^2\alpha_{1nk}}{(1+\nu)(\lambda_n^2+a_k^2)},$$

$$A_{1n2}=\frac{1-e^{b\lambda_n}}{-1+e^{2b\lambda_n}+2be^{b\lambda_n}\lambda_n}\frac{2(-1+\nu)\alpha_{2n0}}{(1+\nu)}$$
$$-\sum_{k=1}^{\infty}\left(\frac{(-1)^k e^{b\lambda_n}(-1+e^{2b\lambda_n}+2b\lambda_n)}{(1-e^{2b\lambda_n})^2-4b^2e^{2b\lambda_n}\lambda_n^2}+\frac{1-e^{2b\lambda_n}-2be^{2b\lambda_n}\lambda_n}{(1-e^{2b\lambda_n})^2-4b^2e^{2b\lambda_n}\lambda_n^2}\right)\frac{2(-1+\nu)\lambda_n^2\alpha_{2nk}}{(1+\nu)(\lambda_n^2+a_k^2)},$$

$$B_{1n1}=\frac{e^{b\lambda_n}(1-e^{b\lambda_n})}{-1+e^{2b\lambda_n}+2be^{b\lambda_n}\lambda_n}\frac{2(-1+\nu)\alpha_{1n0}}{(1+\nu)}$$
$$+\sum_{k=1}^{\infty}\left(\frac{(-1)^k e^{b\lambda_n}(1-e^{2b\lambda_n}-2be^{2b\lambda_n}\lambda_n)}{(1-e^{2b\lambda_n})^2-4b^2e^{2b\lambda_n}\lambda_n^2}+\frac{e^{2b\lambda_n}(-1+e^{2b\lambda_n}+2b\lambda_n)}{(1-e^{2b\lambda_n})^2-4b^2e^{2b\lambda_n}\lambda_n^2}\right)\frac{2(-1+\nu)\lambda_n^2\alpha_{1nk}}{(1+\nu)(\lambda_n^2+a_k^2)},$$

$$B_{1n2}=\frac{e^{b\lambda_n}(1-e^{b\lambda_n})}{-1+e^{2b\lambda_n}+2be^{b\lambda_n}\lambda_n}\frac{2(-1+\nu)\alpha_{2n0}}{(1+\nu)}$$
$$+\sum_{k=1}^{\infty}\left(\frac{(-1)^k e^{b\lambda_n}(1-e^{2b\lambda_n}-2be^{2b\lambda_n}\lambda_n)}{(1-e^{2b\lambda_n})^2-4b^2e^{2b\lambda_n}\lambda_n^2}+\frac{e^{2b\lambda_n}(-1+e^{2b\lambda_n}+2b\lambda_n)}{(1-e^{2b\lambda_n})^2-4b^2e^{2b\lambda_n}\lambda_n^2}\right)\frac{2(-1+\nu)\lambda_n^2\alpha_{2nk}}{(1+\nu)(\lambda_n^2+a_k^2)}.$$

After finding the thermal displacement potential functions, Φ and Ψ, the displacements U, V are determined from the geometric relations:

$$\varepsilon_x=\frac{\partial U}{\partial x},\quad \varepsilon_y=\frac{\partial V}{\partial y},\quad \gamma_{xy}=\frac{1}{2}\left(\frac{\partial U}{\partial y}+\frac{\partial V}{\partial x}\right). \tag{27}$$

Next, thermal stresses may be found from the Duhamel–Neumann relations:

$$\sigma_x=(1-\nu)\varepsilon_x+\nu(\varepsilon_x+\varepsilon_y)-T,\quad \sigma_y=(1-\nu)\varepsilon_y+\nu(\varepsilon_x+\varepsilon_y)-T,\quad \tau_{xy}=\gamma_{xy}. \tag{28}$$

5. Approximated distribution of thermal stresses

5.1. Base functions for nonhomogeneous equations

Equations (23) and (24) (with conditions resulting from conditions (6) to (8) after using substitution (22)) stand for a quasi-static problem. The time τ plays here a role of a parameter. The

problem will be solved by using FEMT. The base functions are defined as a linear combination of T-functions. Functions $\Phi(x,y)$ and $\Psi(x,y)$ are to be found whereas functions $h_1(x,y,\tau)$, $h_2(x,y,\tau)$ are given by (25) and (26). In the equation (23) the function $T(x,y,\tau)$ describes an approximate temperature in the domain Ω for $t=\tau$ which is obtained from measured temperature values in some inner points of the time-space region $\Omega\times<0,\tau>$ (in Sec. 3 the approximate temperature is denoted $\tilde{T}_j(x,y,t)$).

The equations (23) and (24) are nonhomogeneous. The solution of each equation is a sum of a general solution of the homogeneous equation and a particular solution of the nonhomogeneous one.

The domain Ω is divided into rectangular elements Ω_j for $j=1,2,3,\dots J$. In each element Ω_j approximate solutions of the equations (23) and (24) read

$$\tilde{\Phi}_j(x,y)=\sum_{n=1}^{N}A_{jn}v_n(\hat{x},\hat{y})+\tilde{\Phi}_j^{sz}(x,y), \tag{29}$$

$$\tilde{\Psi}_j(x,y)=\sum_{n=1}^{N}B_{jn}v_n(\hat{x},\hat{y})+\tilde{\Psi}_j^{sz}(x,y), \tag{30}$$

where $\hat{x}=x-x_{0j}$, $\hat{y}=y-y_{0j}$, and (x_{0j},y_{0j}) is an arbitrary but fixed point belonging to Ω_j; $v_n(\hat{x},\hat{y})$ stands for harmonic polynomial (T-function for harmonic equation); A_{jn}, B_{jn} are unknown coefficients to be found; $\tilde{\Phi}_j^{sz}(x,y)$ and $\tilde{\Psi}_j^{sz}(x,y)$ stand for particular solutions. The way of finding $\tilde{\Phi}_j^{sz}(x,y)$ and $\tilde{\Psi}_j^{sz}(x,y)$ will be presented in Sec. 5.3.

In Ω_j the nodes with coordinates (x_k,y_k) are chosen. Assuming that values $\tilde{\Phi}_{jn}$ and $\tilde{\Psi}_{jn}$ are known in the nodes we solve the system of algebraic equations ($k=1,2,\dots N$):

$$\tilde{\Phi}_{jk}-\tilde{\Phi}_{jk}^{sz}=\sum_{n=1}^{N}A_{jn}v_n(\hat{x}_k,\hat{y}_k), \tag{31}$$

$$\Psi_{jk}-\tilde{\Psi}_{jk}^{sz}=\sum_{n=1}^{N}B_{jn}v_n(\hat{x}_k,\hat{y}_k), \tag{32}$$

to find A_{jn} and B_{jn}. Here, $\tilde{\Phi}_{jk}^{sz}=\tilde{\Phi}_j^{sz}(x_k,y_k)$, $\tilde{\Psi}_{jk}^{sz}=\tilde{\Psi}_j^{sz}(x_k,y_k)$. In the matrix form they read

$$\mathbf{v}\,\mathbf{A}=\tilde{\mathbf{\Phi}}-\tilde{\mathbf{\Phi}}^{sz}, \tag{33}$$

$$\mathbf{v}\,\mathbf{B}=\tilde{\mathbf{\Psi}}-\tilde{\mathbf{\Psi}}^{sz}, \tag{34}$$

With $\mathbf{V}=\mathbf{v}^{-1}$ we obtain

$$\mathbf{A}=\mathbf{v}^{-1}\big(\tilde{\mathbf{\Phi}}-\tilde{\mathbf{\Phi}}^{sz}\big)=\mathbf{V}\big(\tilde{\mathbf{\Phi}}-\tilde{\mathbf{\Phi}}^{sz}\big),\quad A_{jn}=\sum_{k=1}^{N}V_{nk}\big(\tilde{\Phi}_{jk}-\tilde{\Phi}_{jk}^{sz}\big), \tag{35}$$

$$\mathbf{B}=\mathbf{v}^{-1}\big(\tilde{\mathbf{\Psi}}-\tilde{\mathbf{\Psi}}^{sz}\big)=\mathbf{V}\big(\tilde{\mathbf{\Psi}}-\tilde{\mathbf{\Psi}}^{sz}\big)\quad B_{jn}=\sum_{k=1}^{N}V_{nk}\big(\tilde{\Psi}_{jk}-\tilde{\Psi}_{jk}^{sz}\big). \tag{36}$$

Substituting (35) to (29) we arrive to the following form of the function $\tilde{\Phi}_j$ in j-th element:

$$\begin{aligned}\tilde{\Phi}_j(x,y)&=\sum_{n=1}^{N}\left(\sum_{k=1}^{N}V_{nk}(\tilde{\Phi}_{jk}-\tilde{\Phi}_{jk}^{sz})\right)v_n(\hat{x},\hat{y})+\tilde{\Phi}_j^{sz}(x,y)\\&=\sum_{k=1}^{N}\left(\sum_{n=1}^{N}V_{nk}v_n(\hat{x},\hat{y})\right)(\tilde{\Phi}_{jk}-\tilde{\Phi}_{jk}^{sz})+\tilde{\Phi}_j^{sz}(x,y)\\&=\sum_{k=1}^{N}\varphi_{jk}(x,y)\,(\tilde{\Phi}_{jk}-\tilde{\Phi}_{jk}^{sz})+\tilde{\Phi}_j^{sz}(x,y),\end{aligned} \tag{37}$$

with φ_{jk} (the base functions) defined as follows:

$$\varphi_{jk}(x,y) = \sum_{n=1}^{N} V_{nk} v_n(\hat{x},\hat{y}). \tag{38}$$

Similarly, substituting (36) to (30) we obtain $\tilde{\Psi}_j$:

$$\tilde{\Psi}_j(x,y) = \sum_{k=1}^{N} \varphi_{jk}(x,y)\,(\tilde{\Psi}_{jk} - \tilde{\Psi}^{sz}_{jk}) + \tilde{\Psi}^{sz}_{j}(x,y). \tag{39}$$

5.2. The problem of thermal stresses

To solve approximately the Poisson equations (23) and (24) in Ω a rectangular mesh is introduced. The lines of the mesh are parallel to the axes of the system of coordinates. The sides of the considered rectangle are divided into L_1 parts (the one parallel to OX) and L_2 parts (the one parallel to OY). In each rectangular element Ω_j a set of eight nodes is chosen (see Fig. 6).

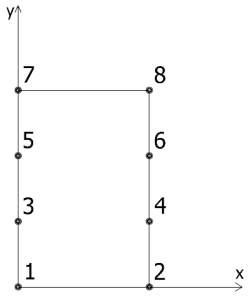

Fig. 6. Eight nodes chosen in an element

Hence, in the domain Ω we have $(L_1+1)(3L_2+1)$ nodes. The base functions, φ_{jk}, are then a linear combination of the following harmonic polynomials:

$$v_1^h(\hat{x},\hat{y}) = 1, \quad v_2(\hat{x},\hat{y}) = \hat{x}, \quad v_3(\hat{x},\hat{y}) = \hat{y}, \quad v_4(\hat{x},\hat{y}) = \hat{x}\,\hat{y},$$

$$v_5(\hat{x},\hat{y}) = \frac{\hat{x}^2}{2} - \frac{\hat{y}^2}{2}, \quad v_6(\hat{x},\hat{y}) = \frac{\hat{x}^3}{6} - \frac{\hat{x}\,\hat{y}^2}{2}, \quad v_7(\hat{x},\hat{y}) = \frac{\hat{x}^2\hat{y}}{2} - \frac{\hat{y}^3}{6}, \quad v_8(\hat{x},\hat{y}) = \frac{\hat{x}^3\hat{y}}{6} - \frac{\hat{x}\hat{y}^3}{6}.$$

To find $\tilde{\Phi}_{jk}$, $\tilde{\Psi}_{jk}$ (unknown values of functions $\tilde{\Phi}_j$, $\tilde{\Psi}_j$ in k-th node of the j-th element) it is more convenient to use global node numeration. The relations (37) and (39) take then for $j = 1,2,\ldots(L_1\,L_2)$, $k = 1,2,\ldots,8$, and $n = 1,2,\ldots,(L_1+1)(3L_2+1)$ the following form:

$$\tilde{\Phi}_j(x,y) = \sum_{k=1}^{8} \varphi_{jk}(x,y)\,(\tilde{\Phi}^n - \tilde{\Phi}^n_{sz}) + \tilde{\Phi}^{sz}_{j}(x,y), \tag{40}$$

$$\tilde{\Psi}_j(x,y) = \sum_{k=1}^{8} \varphi_{jk}(x,y)\,(\tilde{\Psi}^n - \tilde{\Psi}^n_{sz}) + \tilde{\Psi}^{sz}_{j}(x,y). \tag{41}$$

Subscripts j, k and n in (40) and (41) denote the element number, the node number in the j-th element and the node number in Ω, respectively. Moreover, $\tilde{\Phi}^n$ and $\tilde{\Psi}^n$ denote the function $\tilde{\Phi}$ and $\tilde{\Psi}$ values in the n-th node, respectively, $\tilde{\Phi}^{sz}_j(x,y)$ and $\tilde{\Psi}^{sz}_j(x,y)$ stand for the particular solutions

of the equations (23) and (24) in the j-th element, respectively, and $\tilde{\Phi}^n_{sz}$ and $\tilde{\Psi}^n_{sz}$ describe values of the particular solutions in the n-th node.

The searched values $\tilde{\Phi}^n$, $\tilde{\Psi}^n$, i.e., $\tilde{\Phi}$, $\tilde{\Psi}$, approximating values in the n-th node, are found as a result of solving a system of algebraic equations being a result of minimizing the following functional:

$$\begin{aligned} J = {} & W_{P\Phi} + W_{PP\Phi} + W_{P\Psi} + W_{PP\Psi} + W_{B0\,\sigma_y} + W_{B0\,\tau_{xy}} + W_{Bb\,\sigma_y} + W_{Bb\,\tau_{xy}} \\ & + W_{Z\Phi X} + W_{ZP\Phi X} + W_{Z\Phi Y} + W_{ZP\Phi Y} + W_{Z\Psi X} + W_{ZP\Psi X} + W_{Z\Psi Y} + W_{ZP\Psi Y}. \end{aligned} \tag{42}$$

The components of the functional describe inaccuracy of the solution with respect to values of thermal potential functions and their derivatives on both sides of the element borders and inaccuracy of fulfilling the boundary conditions. The component $W_{P\Phi}$ is expressed as follows:

$$W_{P\Phi} = \sum_{n=1}^{L_2} \int_{\frac{n-1}{L_2}b}^{\frac{n}{L_2}b} \left(\tilde{\Phi}_{(n-1)L_1+1}(0,y) - \tilde{\Phi}_{nL_1}(l,y) \right)^2 dy. \tag{43}$$

The rest of components have a similar form.

In the numerical example the Poisson equations have been solved with the use of 400 ($L_1 = 40$, $L_2 = 10$) and 800 ($L_1 = 80$, $L_2 = 10$) rectangular 8-nodal elements. In the case of 400 elements we have 1271 nodes in Ω, for 800 elements the number of nodes enlarges to 2511.

For an approximate solution a relative error was calculated:

$$\text{rel. error} = \sqrt{\frac{\sum_{k=1}^{L} \left(\tilde{f}(x_k, y_k) - f(x_k, y_k) \right)^2}{\sum_{k=1}^{L} \left(f(x_k, y_k) \right)^2}}. \tag{44}$$

Here, $\tilde{f}(x,y)$ stands for the approximate solution, $f(x,y)$ is the exact solution, L denotes the number of nodes, and (x_k, y_k) describes the coordinates of the k-th node.

5.3. Particular solution of a Poisson equation

The problem formulated in the form of equations (23) and (24) is a quasi-static one. Time t is here a parameter. Approximate particular solutions of the equations are then searched for fixed $t = \tau$ in the domain Ω.

The way of finding an approximate solution of a nonhomogeneous equation in the time-space domain is presented in the paper [5]. The approximate form of the particular solutions is described as a linear combination of the biharmonic functions:

$$\tilde{\Phi}^{sz}_j(x,y) = \sum_{n=1}^{N} A_{jn} v_n(\hat{x}, \hat{y}), \tag{45}$$

$$\tilde{\Psi}^{sz}_j(x,y) = \sum_{n=1}^{N} B_{jn} v_n(\hat{x}, \hat{y}). \tag{46}$$

Here, $\hat{x} = x - x_{0j}$ and $\hat{y} = y - y_{0j}$, (x_{0j}, y_{0j}) is an arbitrary but fixed point in Ω_j, $v_n(\hat{x}, \hat{y})$ denote the n-th biharmonic functions [3, 5], A_{jn} and B_{jn} stand for the unknown coefficients.

In the elements Ω_j the number of nodes is equal to the number of T-functions used. The base functions φ_{jk} are constructed in the same way as in Sec. 3. The approximate particular solutions are then expressed as linear combinations of the base functions:

$$\tilde{\Phi}^{sz}_j(x,y) = \sum_{k=1}^{N} \varphi_{jk}(x,y)\, \tilde{\Phi}^n_{sz}, \tag{47}$$

$$\tilde{\Psi}_j^{sz}(x,y) = \sum_{k=1}^{N} \varphi_{jk}(x,y)\, \tilde{\Psi}_{sz}^{n}. \tag{48}$$

Subscripts j, k and n in Eqs. (47) and (48) denote the element number, the node number in the j-th element and the node number in Ω, respectively. Moreover, $\tilde{\Phi}_{sz}^{n}$ and $\tilde{\Psi}_{sz}^{n}$ describe the unknown values of the particular solutions in the n-th node.

In order to find the unknowns, the following two functionals are minimized:

$$J_\Phi = W_\Phi + W_{Z\Phi X} + W_{ZP\Phi X} + W_{Z\Phi Y} + W_{ZP\Phi Y}, \tag{49}$$

$$J_\Psi = Z_\Psi + W_{Z\Psi X} + W_{ZP\Psi X} + W_{Z\Psi Y} + W_{ZP\Psi Y}. \tag{50}$$

Components of the functionals have similar meaning to those used in building the functional J in the formula (42). They are expressed as follows:

$$W_\Phi = \sum_{n=1}^{L_2}\sum_{m=1}^{L_1} \int_{\frac{m-1}{L_1}l}^{\frac{m}{L_1}l} \int_{\frac{n-1}{L_2}b}^{\frac{n}{L_2}b} \left(\frac{\partial^2 \Phi_{m+(n-1)L_1}^{sz}}{\partial\, x^2} + \frac{\partial^2 \Phi_{m+(n-1)L_1}^{sz}}{\partial\, y^2} - \big(h_1(x,y) + T(x,y,\tau)\big) \right)^2 dy\, dx,$$

$$W_{Z\Phi X} = \sum_{n=1}^{L_2}\sum_{m=1}^{L_1-1} \int_{\frac{n-1}{L_2}b}^{\frac{n}{L_2}b} \left(\Phi_{m+(n-1)L_1}^{sz}\Big(\frac{m}{L_1}l, y\Big) - \Phi_{m+1+(n-1)L_1}^{sz}\Big(\frac{m}{L_1}l, y\Big) \right)^2 dy,$$

$$W_{Z\Phi Y} = \sum_{n=1}^{L_2-1}\sum_{m=1}^{L_1} \int_{\frac{m-1}{L_1}l}^{\frac{m}{L_1}l} \left(\Phi_{m+(n-1)L_1}^{sz}\Big(x, \frac{n}{L_2}b\Big) - \Phi_{m+nL_1}^{sz}\Big(x, \frac{n}{L_2}b\Big) \right)^2 dx,$$

$$W_{ZP\Phi Y} = \sum_{n=1}^{L_2-1}\sum_{m=1}^{L_1} \int_{\frac{m-1}{L_1}l}^{\frac{m}{L_1}l} \left(\frac{\partial \Phi_{m+(n-1)L_1}^{sz}}{\partial y}\Big(x, \frac{n}{L_2}b\Big) - \frac{\partial \Phi_{m+nL_1}^{sz}}{\partial y}\Big(x, \frac{n}{L_2}b\Big) \right)^2 dx,$$

$$W_\Psi = \sum_{n=1}^{L_2}\sum_{m=1}^{L_1} \int_{\frac{m-1}{L_1}l}^{\frac{m}{L_1}l} \int_{\frac{n-1}{L_2}b}^{\frac{n}{L_2}b} \left(\frac{\partial^2 \Psi_{m+(n-1)L_1}^{sz}}{\partial\, x^2} + \frac{\partial^2 \Psi_{m+(n-1)L_1}^{sz}}{\partial\, y^2} - h_2(x,y) \right)^2 dy\, dx,$$

$$W_{Z\Psi X} = \sum_{n=1}^{L_2}\sum_{m=1}^{L_1-1} \int_{\frac{n-1}{L_2}b}^{\frac{n}{L_2}b} \left(\Psi_{m+(n-1)L_1}^{sz}\Big(\frac{m}{L_1}l, y\Big) - \Psi_{m+1+(n-1)L_1}^{sz}\Big(\frac{m}{L_1}l, y\Big) \right)^2 dy,$$

$$W_{ZP\Psi X} = \sum_{n=1}^{L_2}\sum_{m=1}^{L_1-1} \int_{\frac{n-1}{L_2}b}^{\frac{n}{L_2}b} \left(\frac{\partial \Psi_{m+(n-1)L_1}^{sz}}{\partial x}\Big(\frac{m}{L_1}l, y\Big) - \frac{\partial \Psi_{m+1+(n-1)L_1}^{sz}}{\partial x}\Big(\frac{m}{L_1}l, y\Big) \right) dy,$$

$$W_{Z\Psi Y} = \sum_{n=1}^{L_2-1}\sum_{m=1}^{L_1} \int_{\frac{m-1}{L_1}l}^{\frac{m}{L_1}l} \left(\Psi_{m+(n-1)L_1}^{sz}\Big(x, \frac{n}{L_2}b\Big) - \Psi_{m+nL_1}^{sz}\Big(x, \frac{n}{L_2}b\Big) \right)^2 dx,$$

$$W_{ZP\Psi Y} = \sum_{n=1}^{L_2-1} \sum_{m=1}^{L_1} \int_{\frac{m-1}{L_1}l}^{\frac{m}{L_1}l} \left(\frac{\partial \Psi^{sz}_{m+(n-1)L_1}}{\partial y}\Big(x, \frac{n}{L_2}b\Big) - \frac{\partial \Psi^{sz}_{m+nL_1}}{\partial y}\Big(x, \frac{n}{L_2}b\Big) \right)^2 dx.$$

The unknown coefficients Φ^n_{sz} and Ψ^n_{sz} are the solutions of two systems of algebraic equations being a result of minimizing the functionals J_Φ and J_Ψ. The approximate particular solutions are then used in Sec. 5.1 to find the approximate solutions of equations (23) and (24).

In the considered problem the domain Ω has again been divided into 400 ($L_1 = 40$, $L_2 = 10$) and 800 ($L_1 = 80$, $L_2 = 10$) rectangular 8-nodal elements. The base functions are built as a linear combination of the following eight biharmonic functions:

$$v_1(\hat{x},\hat{y}) = 1, \qquad v_2(\hat{x},\hat{y}) = \hat{x}, \qquad v_3(\hat{x},\hat{y}) = \hat{y}, \qquad v_4(\hat{x},\hat{y}) = \hat{x}\,\hat{y},$$
$$v_5(\hat{x},\hat{y}) = \frac{\hat{x}^2+\hat{y}^2}{4}, \quad v_6(\hat{x},\hat{y}) = \frac{\hat{x}^3}{12} + \frac{\hat{x}\,\hat{y}^2}{4}, \quad v_7(\hat{x},\hat{y}) = \frac{\hat{x}^2\hat{y}}{4} + \frac{\hat{y}^3}{12}, \quad v_8(\hat{x},\hat{y}) = \frac{\hat{x}\,\hat{y}^3}{12} + \frac{\hat{x}^3\hat{y}}{12}.$$

6. Numerical example

In the numerical example the following data are used: $\bar{v}_s = 0.02\ \frac{\mathrm{m}}{\mathrm{s}}$, $\tau = 2.27$ s, $\bar{T}_0 = 293$ K, $\bar{l} = 0.3$ m, $\bar{b} = 0.03$ m, $\bar{a} = 0.09$ m, $\kappa = 0.119 \cdot 10^{-4}\ \frac{\mathrm{m}^2}{\mathrm{s}}$, $\lambda = 45\ \frac{\mathrm{W}}{\mathrm{m\,K}}$, $Q = 13 \cdot 10^4$, $\nu = 0.3$, $\mu = 81 \cdot 10^6\ \frac{\mathrm{kN}}{\mathrm{m}^2}$, $\alpha_t = 12 \cdot 10^{-6}\ \frac{1}{\mathrm{K}}$. Graphs presented in Figs. 7(a), 8(a) and 9(a) are generated for the case of 800 elements ($L_1 = 80$, $L_2 = 10$). The exact values of stresses are shown in Figs. 7(b), 8(b) and 9(b).

When comparing Figs. 7(a) and 7(b), one can notice a good consistence of both graphs (see also Table 2). The approximate values of stresses σ_x (parallel to the longer side of the rectangle) change in the range from minus 20000 $\frac{\mathrm{kN}}{\mathrm{m}^2}$ to plus 4000 $\frac{\mathrm{kN}}{\mathrm{m}^2}$. The greatest absolute value of the stress is situated just under the acting heat source and represents compressive stress.

In the case of stresses σ_y, perpendicular to the longer side of the rectangle, the results of the approximate solution are much worse than those obtained for σ_x (see Table 2). In the case of 800

Table 2. Relative error values for the stresses σ_x, σ_y, and τ_{xy}

Stresses	Relative error [%], Eq. (44)	
	400 elements $L = 1271$	800 elements $L = 2511$
σ_x	4.53	3.95
σ_y	40	26
τ_{xy}	35.3	12.1

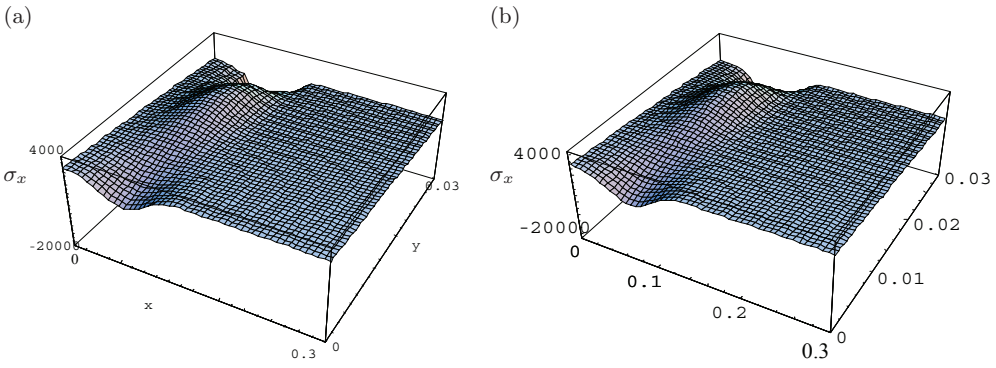

Fig. 7. Approximate (a) and exact (b) distribution of the normal stresses σ_x $[\frac{\mathrm{kN}}{\mathrm{m}^2}]$

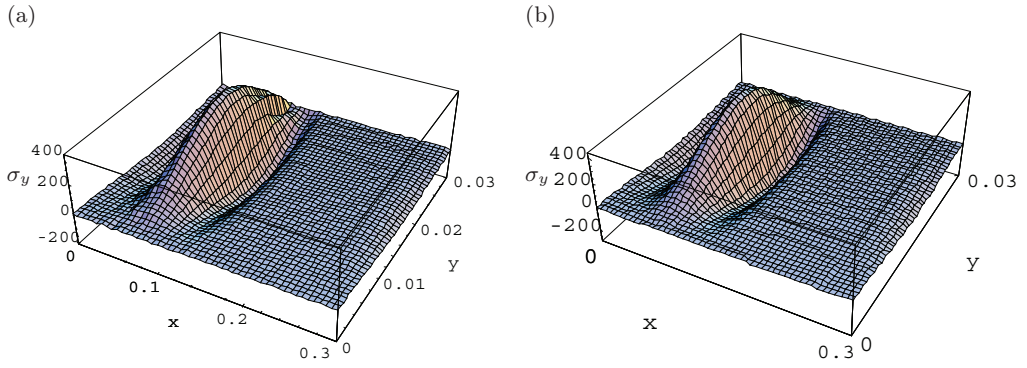

Fig. 8. Approximate (a) and exact (b) distribution of the normal stresses σ_y $[\frac{\mathrm{kN}}{\mathrm{m}^2}]$

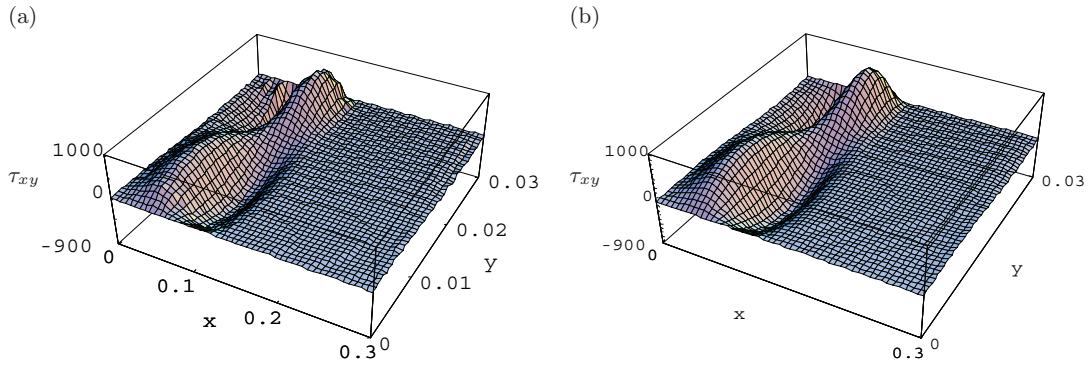

Fig. 9. Approximate (a) and exact (b) distribution of the tangential stresses τ_{xy} $[\frac{\mathrm{kN}}{\mathrm{m}^2}]$

elements the relative error is equal to 26%. It is probably a result of the considered mesh (80 elements in the directions OX and only 10 elements in the direction OY). However, the character and extreme values of the stresses are almost the same on both graphs presented in Fig. 8. A big relative error is probably caused by the "waving" of the obtained approximate solution. Because the values of these stresses are small comparing to σ_x, the results seems to be acceptable.

In the case of tangential stresses one can notice an acceptable consistence of both graphs (see also Table 2). The character and extreme values of the stresses are almost the same on both graphs, which is well presented on the contour graphs.

7. Final remarks

Because of the limitations of hardware used for calculation the considered region was divided into the simplest 8-nodal cuboid or rectangular elements with nodes at the corners. The base functions then consist of eight components and therefore we have a low degree approximation which is better for numerical conditioning of the problem. However, it is possible to introduce a different set of nodes and different shapes of the finite elements.

The presented example shows that the T-functions for heat conduction and for harmonic equations are suitable to construct the time-space (or spatial) shape functions in the FEMT in order to identify the temperature and thermal stresses in the considered domain based on the values of temperature measured inside the body when it is heated by a moving heat source. The presented analysis concerns a rectangular body but it is obvious that such approach can be applied to bodies of more complicated shape.

We conducted many numerical experiments with different numbers of finite elements in the time-space (and spatial) region, up to 800. The obtained approximate solution seems to be acceptable or at least promising. However, for the heat source moving along the boundary with velocity greater than the one considered in the paper it is absolutely necessary to introduce greater number of the time-space (and spatial, respectively) elements. Similarly, the smaller size of the moving heat source is (independently of its velocity) the denser division of the region ought to be applied to obtain a satisfactory solution.

Acknowledgements

This work was carried out in the framework of the research project No N513 003 32/0541, which was financed from the resources for the development of science in the years 2007-2009.

References

[1] M. Ciałkowski. Treffz functions as basis functions of FEM in application to solution of inverse heat conduction problem. *Computer Assisted Mechanics and Engineering Sciences*, **8**: 247–260, 2001.

[2] M. Ciałkowski, Solution of inverse heat conduction problem with use new type of fnite element base functions. In: B.T. Maruszewski, W. Muschik A. Radowicz (eds.), *Proceedings of the International Symposium on Trends in Continuum Physics*. World Scientifc Publishing, Singapore, New Jersey, London, Hong Kong, pp. 64–78, 1999.

[3] M. Ciałkowski, A. Frąckowiak. *Heat functions and their application to solving heat conduction and mechanical problems* (in Polish). Wydawnictwo Politechniki Poznańskiej, Poznań, 2000.

[4] M. Ciałkowski, A. Frąckowiak. Solution of the stationary 2D inverse heat conduction problem by Trefftz Method. *Journal of Thermal Science*, **11**(2): 148–162, 2002.

[5] M. Ciałkowski, A. Frąckowiak. Heat functions and related in solving chosen equations of mechanics. Part I. Solving some differential equations using the inversion operations (in Polish). *Studia i Materiały. Technika 3*, pp. 7–69, Uniwersytet Zielonogórski, Zielona Góra, 2003.

[6] M. Ciałkowski, A. Frąckowiak, K. Grysa. Physical regularization for inverse problems of stationary heat conduction. *J. Inv. Ill-Posed Problems*, **15**: 1–18, 2007.

[7] M. Ciałkowski, A. Frąckowiak, J. Kołodziej. Investigation of laminar flow through solution of inverse problem for heat conduction equation. *Mechanics Research Communications*, **28**(6): 623–628, 2001.

[8] M. Ciałkowski, S. Futakiewicz, L. Hożejowski. Method of heat polynomials in solving the inverse heat conduction problems. *ZAMM*, **79**: 709–710, 1999.

[9] M. Ciałkowski, S. Futakiewicz, L. Hożejowski. Heat polynomials applied to direct and inverse heat conduction problems. In: B.T. Maruszewski, W. Muschik A. Radowicz (eds.), *Proceedings of the International Symposium on Trends in Continuum Physics*. World Scientifc Publishing, Singapore, New Jersey, London, Hong Kong, pp. 79–88, 1999.

[10] B.H. Dennis, G.S. Dulikravich, S. Yoshimura. A Finite Element Formulation for the Determination of Unknown Boundary Conditions for 3-D Steady Thermoelastic Problems. *ASME Journal of Heat Transfer*, **126**(1): 110–119, 2004.

[11] K. Grysa, B. Maciejewska. Application of the modified finite elements method to identification of moving heat source. In: A. Nowak, R. Białecki, G. Węcel (eds.), *EUTOTERM 82, Numerical Heat Transfer 2005*, Vol. 2, pp. 493–502, Gliwice–Kraków, Poland, Sept. 13–16, 2005.

[12] L. Hożejowski, S. Hożejowska, M. Sokała. Stability of solutions for some inverse heat conduction problems by heat functions method. *Journal of Applied Mathematics and Mechanics ZAMM*, **81**: 499–500, 2001.

[13] L. Hożejowski, S. Hożejowska, M. Sokała. Evaluation of the Biot number with the use of heat functions. *Proc. Appl. Math. Mech.*, **1**: 349–350, 2002.

[14] B. Kruk, M. Sokała. Sensitivity coeffcients and heat polynomials in the inverse heat conduction problems. *ZAMM*, **80**(Supplement 3): 693–694, 2000.

[15] B. Kruk, M. Sokała. Sensitivity coeffcients applied to two-dimensional transient inverse heat conduction problems. *ZAMM*, **81**(Supplement 4): 945–946, 2001.

[16] B. Kruk, M. Sokała. Beck's procedure – sensitivity of the algorithm to measurement error. *Proc. Appl. Math. Mech.*, **2**: 370–371, 2003.

[17] A. Maciąg. *Trefftz functions for chosen direct and inverse problems of mechanics* (in Polish). Wydawnictwo Politechniki Świętokrzyskiej, Kielce, 2009.

[18] B. Maciejewska. The transient temperature field in a rectangular area with movable heat sources at its edge. *JTAM*, **42**(4): 789–804, 2004.

[19] W. Nowacki. *Teoria sprężystości*. PWN, Warszawa, 1970.
[20] M. Piasecka, S. Hożejowska, M.E. Poniewski. Determination of local flow boiling heat transfer coeffcient in narrow channel, *Archives of Thermodynamics*, **24**(2): 55–67, 2003.
[21] M. Piasecka, S. Hożejowska, M.E. Poniewski. Experimental evaluation of flow boiling incipience of subcooled uid in a narrow channel. *International Journal of Heat and Fluid Flow*, **25**(2): 159–172, 2004.
[22] J. Taler. Analytical solution of the overdetermined inverse heat conduction problem with an application to monitoring thermal stresses. *Heat and Mass Transfer*, **33**: 209–218, 1997.
[23] A.K. Tikhe, K.C. Deshmukh. *Inverse transient thermoelastic deformations in thin circular plates. Sadhana*, **30**(5): 661–671, 2005.
[24] Yu-Ching Yang, Un-Chia Chen, Win-Jin Chang. An inverse problem of coupled thermoelasticity in predicting heat flux and thermal stresses by strain measurement. *Journal Of Thermal Stresses*, **25**(3): 265–281, 2002.
[25] R.M. Kushnir, A.V. Yasinskyi. Identification of the temperature field and stresses in a thermosensitive cylinder according to the surface strains. *Materials Science*, **43**(6): 814–822, 2007.
[26] M. Bonnet, A. Constantinescu. Inverse problems in elasticity. *Inverse Problems*, **21**: R1–R50, 2005.